Materials Science Forum Vols. 558-559 (2007) pp. 915-920
online at http://www.scientific.net

Three-Dimensional Microstructure Reconstruction Using FIB-OIM

S.-B. Lee [a], A. D. Rollett [b], and G. S. Rohrer [c]

Department of Materials Science & Engineering, Carnegie Mellon University,
Pittsburgh, PA 15213, U. S. A.

[a]sukbin@andrew.cmu.edu, [b]rollett@andrew.cmu.edu, [c]gr20@andrew.cmu.edu

Keywords: Focused Ion Beam-Orientation Imaging Microscopy (FIB-OIM), Electron Back Scatter Diffraction (EBSD), Serial Sectioning, Disorientation, Normalized Grain Size Distribution

Abstract. A new method for reconstructing a three-dimensional microstructure using the focused ion beam-orientation imaging microscopy (FIB-OIM) is introduced. The technique is important for the study of three-dimensional microstructures of materials because it can automatically align (register) a series of parallel sections with both topological information and orientation information at the sub-micrometer scale. Using voxel-based tessellation, a three-dimensional microstructure is reconstructed by registering each section. The application of the method to a cubic material is described and, based on the reconstruction, the grain shape and grain size distribution are characterized.

Introduction

Materials characterization is a crucial step in exploring microstructure-property relationships and, because of the opacity of most crystalline materials, it is conventionally based on data obtained from two-dimensional plane sections. Many problems related to the properties of materials such as corrosion, fatigue crack formation and fracture are three-dimensional in nature because most practical materials have a polycrystalline structure with tremendous complexity in the spatial arrangement of the microstructural units (grains, grain boundaries, orientations, particles and so on). Clearly, conventional two-dimensional characterization is not always sufficient to quantitatively describe the microstructure. Even though stereology can be used to deduce the three-dimensional microstructure from two-dimensional observations, its statistical approach inevitably requires various spatial and morphological assumptions about the defect structure [1].

Considerable effort has been made to reconstruct three-dimensional microstructures using serial sectioning in recent years [2-6]. Saylor et al. [2] have used serial sections to determine grain boundary energies over all five crystallographic parameters. Others have reconstructed microstructures while either automating the sectioning using the techniques based on the focused ion beam [4, 5] or using local orientation information obtained from a series of EBSD maps [6]. Recently, a new automated serial sectioning method for reconstructing three-dimensional microstructures using the focused ion beam-orientation imaging microscopy (FIB-OIM) was developed, giving a full description of both morphology and local orientation of the microstructures

in three dimensions [7-10]. In this paper, we introduce an example of a reconstruction based on the registration of a set of electron back-scatter diffraction (EBSD) images acquired in a dual-beam instrument that combines ion beam milling with a scanning electron microscope. We then present selected characteristics of the reconstructed microstructure including grain morphology and grain size distribution.

Reconstruction Procedure

The figure below shows the EBSD maps of two adjacent layers from a series of cross-sections of a Ni-based alloy obtained through serial sectioning in a dual-beam system. The data was collected and provided by Air Force Research Laboratory (AFRL) using the FEI system. The number of serial sections was 96 and the area of each scanned section was about 50^2 μm^2. For both figures, the black and speckled regions represent the collection of scanned pixels where the EBSD system attempted to index a diffraction pattern but was not able to produce a solution. The central region with well-indexed points shows that a registration system based on orientation information must take into account the local quality of the data available. As illustrated in Fig. 1, the position of the region of reliable data did not remain constant from layer-to-layer. For the TSL system used in this instance, there are two indicators of quality, which are known as “confidence index” (CI) and “image quality” (IQ). CI varies between -1 (poor) and 1 (good) and experience suggests that values above about 0.1 are reliable. Examination of the IQ values for this specific example suggested that poorly indexed pixels had the IQ values smaller than 100.

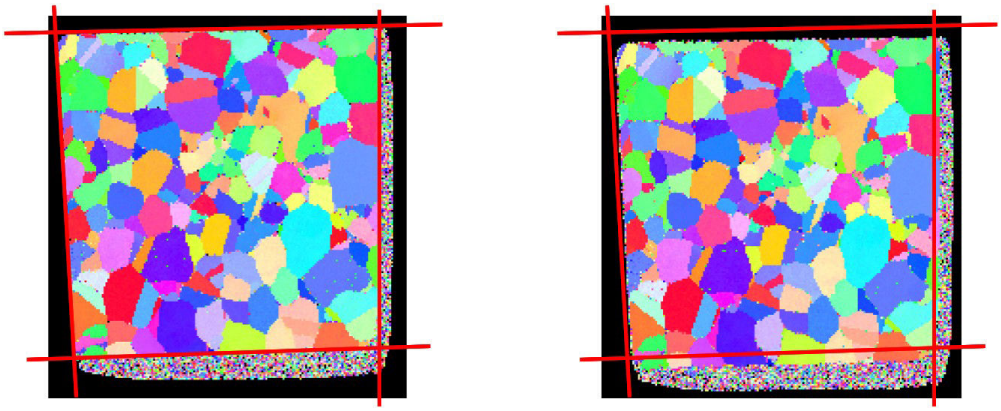

Fig. 1. Inverse pole figure maps of two adjacent sections of a nickel-based alloy. The thick red lines illustrate the edges of the area with reliable data (left figure). Notice that the abrupt deviation of the area of reliable data in the next layer (right figure) from the thick red lines indicates how each layer drifts laterally during the milling and EBSD mapping.

The registration was based on the assumption that the successive layers were sufficiently well aligned that the only adjustment required was the translation confined to integer valued shifts along x and y directions in each plane (i.e. the layers could be assumed to be parallel to one another, with no rotations between layers). We used the orientation information inherent in the EBSD maps to

align the successive layers, which exhibited significant displacements relative to one another (See the figure above). The average disorientation (D) was calculated as shown in Eq. 1 as the average of the product of disorientation, Δg, between each well-indexed pixel in the upper layer and its one or more neighboring pixels in the layer below and a weighting factor, w, that decreases the contribution to D from points in the layer below having a low confidence index and low image quality. The expectation is that good alignment will generate a small average disorientation between pixels in adjacent layers.

$$D = \frac{1}{N}\sum_i w_i \Delta g_i, \quad \begin{cases} w_i = 1, & if\ CI_{neigh} \geq 0.1\ and\ IQ_{neigh} \geq 100 \\ w_i = (2.0 - 10.0 \times CI_{neigh}), & otherwise \end{cases} \tag{1}$$

The figure 2 illustrates the result of using this algorithm on a particular pair of adjacent layers. The number of neighboring pixels contributing to the calculation of average disorientation was one for this case. Notice that a sharp minimum exists in the average disorientation as a function of translations along x and y directions, which permits a particular (*dx, dy*) translation to be used to register the two layers.

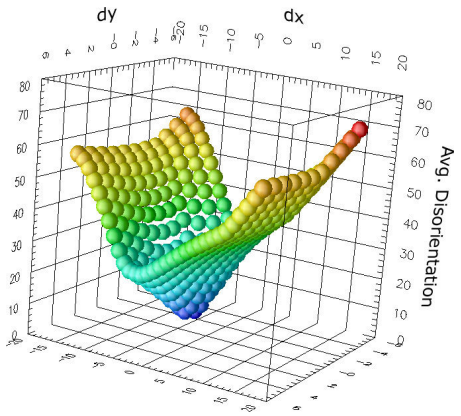

Fig. 2. Average disorientation per pixel in a layer as a function of the translation in x and y of the layer below. The number of nearest neighboring pixels included in the calculation of Eq. (1) is one. The units of translation and average disorientation are pixels and degrees, respectively. Note that, for a particular alignment of the two layers, a well-defined minimum exists.

Results

1. Reconstructed 3D Microstructure and Grains

Figure 3 illustrates the result of applying the above algorithm to the complete set of 96 layers of a Ni-based alloy. After registration, a clean-up procedure was applied in which the grains smaller than 30 voxels in volume were absorbed into their neighbor grains. This cutoff size (30 voxels) was carefully chosen such that the grains eliminated were smaller than the smallest grains associated with the dominant size distribution. These small ‘grains’ were assumed to be either second phase

particles or poorly indexed points. Because of the relatively low stacking fault energy in this alloy, a high density of annealing twins was present in the material, which are evident as straight boundary traces in the sections. It was observed that most of the reconstructed annealing twins in the cross sections of the aligned structure also exhibited straight, flat sides, which suggests that the registration procedure was reasonably successful.

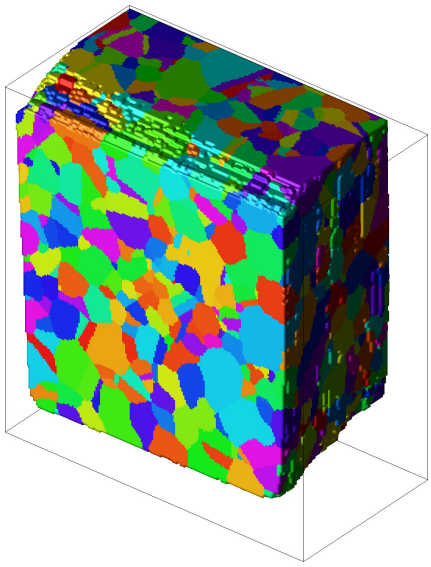

Fig. 3. Aligned 3D digital microstructure obtained by registering the layers with an objective function based on average disorientation between neighboring pixels in adjacent layers. In addition to registration, a clean-up of the grains smaller than a cutoff value has been performed.

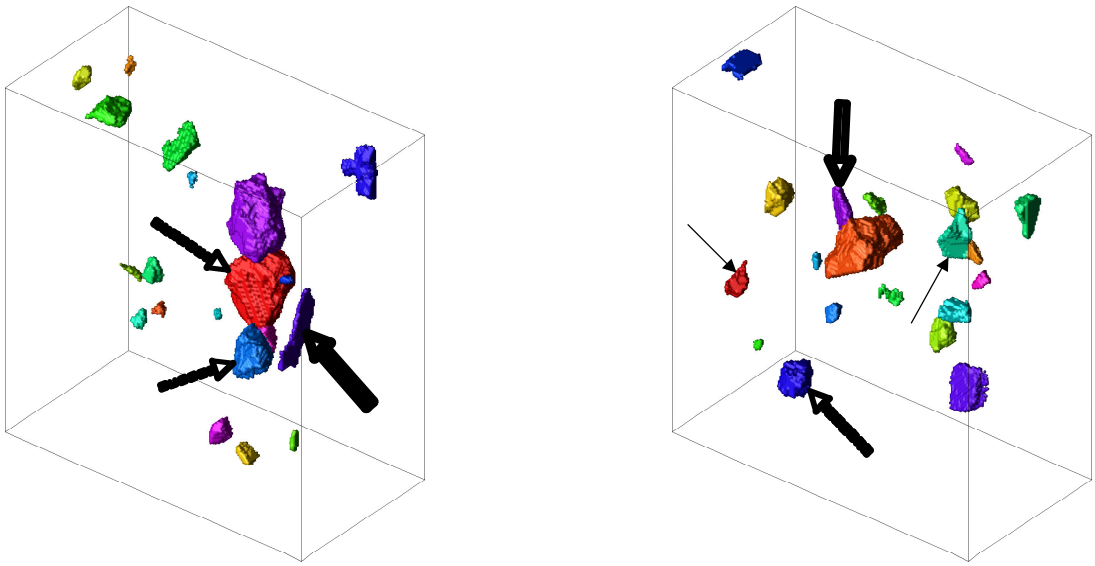

Fig. 4. Morphologies of selected grains in the 3D reconstructed microstructure. The individual grains were illustrated using different colors. Note that the morphologies are 1) equiaxed (marked with dashed arrows), 2) plate-like (annealing twins, marked with bold arrows) or 3) straight, flat sided (marked with thin arrows), suggesting that the alignment algorithm worked reasonably well.

3D Morphologies of the grains were examined by visualizing randomly selected grains to make sure that the proposed algorithm worked reasonably well. In Fig. 4, it is evident that the reconstructed microstructure contains 1) equiaxed bulk grains (marked with dashed arrows), 2) straight, flat-sided grains (marked with thin arrows) and 3) plate-like annealing twins (marked with bold arrows), again suggesting that the alignment was successful.

2. Grain Size Distribution

The grain size distribution corresponding to the reconstructed microstructure in Fig. 3 was obtained using the normalized equivalent spherical radius, $R/\langle R\rangle$, where $\langle R\rangle$ is the average radius of grains. The grains adjacent to the edge of the reconstructed region were excluded from the calculation and the total number of bulk grains was 1018. The result and its comparison with the grain size distributions from both 3D Monte Carlo (MC) simulation of normal grain growth and a 3D reconstruction of a polycrystalline iron [11] are shown in Fig. 5. It has been reported [12-14] that MC simulation accurately simulates the grain growth phenomenon. With the assumption that MC algorithm gives a reasonable grain size distribution and considering the fact that the microstructure generated from the 3D MC normal grain growth simulation does not incorporate annealing twins, the shift towards the lower end of the grains size distribution of the reconstructed microstructure with a longer tail at large sizes may be a consequence of the presence of a high density of annealing twins in the reconstructed microstructure.

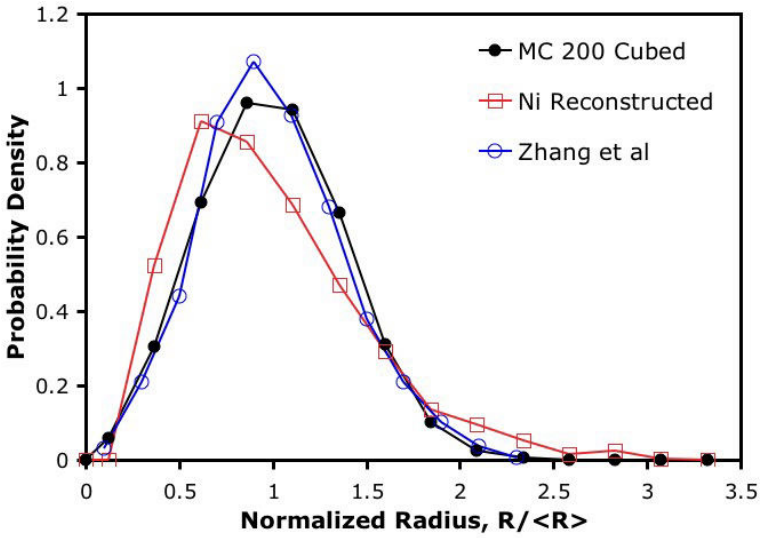

Fig. 5. Normalized size distribution of the bulk grains in the reconstructed microstructure (shown in Fig. 3), compared with the results from both 3D normal grain growth simulation using Monte Carlo algorithm and a 3D experimental data obtained from a polycrystalline iron [11].

Conclusion

A set of EBSD maps of serial sections of a Ni-based alloy obtained using focused ion beam-orientation imaging microscopy (FIB-OIM) was investigated. The alignment of the sections was

performed by minimizing an objective function that exploits the local orientation information inherent in the EBSD maps by calculating the average disorientation between adjacent layers. The reconstructed 3D morphologies of the individual grains and twin boundaries, and grain size distribution suggest that the proposed alignment algorithm was reasonably successful.

Acknowledgements

The authors would like to thank Dr. Michael D. Uchic at Air Force Research Laboratory (AFRL) for providing the serial sectioned data of a Ni-based alloy. This work was supported primarily by the MRSEC program of the National Science Foundation under Award Number DMR-0520425. Partial support from the Pennsylvania DCEC is also acknowledged.

References

[1] E. Underwood: *Quantitative Stereology*. New York: Addison-Wesley (1970)

[2] D. M. Saylor, B, S, El-Dasher, B. L. Adams and G. S. Rohrer: Metallurgical and Materials Transactions 35A, p.1981 (2004)

[3] H. Schaeben, M. Apel, T. Frank, M. Iwanowski, S. Zaefferer in: *Icotom 14: Textures Of Materials, Pts 1and 2*, p.185 (2005)

[4] M. D. Uchic, M. A. Groeber, D. M. Dimiduk and J. P. Simmons: Scripta Materialia 55, p.23 (2006)

[5] B. Maruyama, J. E. Spowart, D. J. Hooper, H. M. Mullens and A. M. Druma: Scripta Materialia 54, p.1709 (2006)

[6] D. J. Rowenhorst, A. Gupta, C. R. Feng and G. Spanos: Scripta Materialia 55, p.11 (2006)

[7] S. Zaefferer: Mater Sci Forum 495-497, p.3 (2005)

[8] J. Conrad, S. Zaefferer and D. Raabe: Acta Mater. 54(5), p.1369 (2006)

[9] M. Groeber, Y. Bhandari, M. D. Uchic, D. M. Dimiduk and S. Chosh: Microsc Microanal 11, p.1626 (2005)

[10] M. D. Uchic, M. Groeber, R. Wheeler IV, F. Scheltens and D. M. Dimiduk: Microsc Microanal 10, p.1136 (2004)

[11] C. Zhang, A. Suzuki, T. Ishimaru, and M. Enomoto: Metall. Mater. Trans, 35A, p.1927 (2004)

[12] M. P. Anderson, D. J. Srolovitz, G. S. Grest and P. S. Sahni: Scripta Metall. 32(5), p.783 (1984)

[13] M. P. Anderson, G. Grest and D. J. Srolovitz (1989): Phil. Mag. B 59(3), p.293 (1989)

[14] A. D. Rollett, D. J. Srolovitz and M. P. Anderson: Acta Metall. 37(4), p.1227 (1989)